TECHNICAL REPORT BRL-TR-3244

BRL

A METHOD FOR EXTRACTING THE SABOT DISCARD IMPULSE FROM TRANSITIONAL BALLISTIC DATA

PETER PLOSTINS

JUNE 1991

U.S. ARMY LABORATORY COMMAND

BALLISTIC RESEARCH LABORATORY
ABERDEEN PROVING GROUND, MARYLAND

NOTICES

Destroy this report when it is no longer needed. DO NOT return it to the originator.

Additional copies of this report may be obtained from the National Technical Information Service, U.S. Department of Commerce, 5285 Port Royal Road, Springfield, VA 22161.

The findings of this report are not to be construed as an official Department of the Army position, unless so designated by other authorized documents.

The use of trade names or manufacturers' names in this report does not constitute indorsement of any commercial product.

REPORT DOCUMENTATION PAGE

Form Approved
OMB No. 0704-0188

1. AGENCY USE ONLY (Leave blank)	2. REPORT DATE	3. REPORT TYPE AND DATES COVERED
	June 91	Final Jan 90 - Dec 90

4. TITLE AND SUBTITLE
A Method for Extracting the Sabot Discard Impulse From Transitional Ballistic Data

5. FUNDING NUMBERS
1L162618AH80

6. AUTHOR(S)
Peter Plostins

7. PERFORMING ORGANIZATION NAME(S) AND ADDRESS(ES)
US Army Ballistic Research Laboratory
ATTN: SLCBR-LF-F
Aberdeen Proving Ground, MD 21005-5066

8. PERFORMING ORGANIZATION REPORT NUMBER

9. SPONSORING/MONITORING AGENCY NAME(S) AND ADDRESS(ES)
US Army Ballistic Research Laboratory
ATTN: SLCBR-DD-T
Aberdeen Proving Ground, MD 21005-5066

10. SPONSORING/MONITORING AGENCY REPORT NUMBER
BRL-TR-3244

11. SUPPLEMENTARY NOTES

12a. DISTRIBUTION/AVAILABILITY STATEMENT
Approved for public release;
distribution is unlimited.

12b. DISTRIBUTION CODE

13. ABSTRACT (Maximum 200 words)

A model is proposed describing the linear and angular motion of a kinetic energy penetrator during the sabot discard. It is based on the equations governing the planar free-flight motion of a symmetric missile with an added impulsive loading. The model is incorporated into a non-linear least-squares fitting routine that is used to fit transitional ballistic data and extract the magnitude, direction, and duration of the sabot discard disturbances. Transitional ballistic data for a 120 mm sabot/penetrator projectile is fitted and the results indicate the model adequately captured the basic physics of the impulsive sabot discard disturbances. The information on the impulsive discard forces can be used to design future sabot/penetrator launch systems.

14. SUBJECT TERMS	15. NUMBER OF PAGES
kinetic energy projectiles; sabots; KE ammunition jump; sabot discard	19
	16. PRICE CODE

17. SECURITY CLASSIFICATION OF REPORT	18. SECURITY CLASSIFICATION OF THIS PAGE	19. SECURITY CLASSIFICATION OF ABSTRACT	20. LIMITATION OF ABSTRACT
UNCLASSIFIED	UNCLASSIFIED	UNCLASSIFIED	Same as Report

INTENTIONALLY LEFT BLANK.

ACKNOWLEDGMENTS

Hearty appreciation is extended to Mr. J.W. Bradley and Mr. John Kietzman for their patient efforts in debugging this application of the non-linear least-squares fitting routine.

INTENTIONALLY LEFT BLANK.

TABLE OF CONTENTS

INTENTIONALLY LEFT BLANK.

LIST OF FIGURES

INTENTIONALLY LEFT BLANK.

I. INTRODUCTION

An important factor determining the launch precision of a long-rod penetrator is the mechanical and aerodynamic disengagement of the sabot petals during the transitional ballistic launch phase. For certain sabot/penetrator systems, as much as one-third of the jump and dispersion can be attributed directly to the mechanical interaction. As long-rod penetrators increase in length, thus requiring longer and more flexible sabot petals, the discard interaction is amplified. The mechanical disengagement point moves away from the penetrator center of gravity, increasing the magnitude of asymmetric angular disturbances. The longer rear sabot ramps are flexible structural members and bend significantly prior to lift-off. Mechanical damage to the sabot petals has been observed and in radical cases sabot rear ramps have broken during the discard phase. Bending of the rear sabot ramp is evident in the photographic data presented in Reference (1). Aerodynamic disturbances generally are observed when asymmetric shock waves from the blunt sabot petals pass over the penetrator fins. Reference (2) presents evidence of the aerodynamic interaction.

An understanding of the qualitative and quantitative aspects of the sabot disengagement phenomenon is required in order to improve the launch dynamics and dynamic structural design of sabot petals. Transitional ballistic yaw and trajectory data can be obtained by techniques described in Reference (3). These data contain the effects of the mechanical and aerodynamic disturbances; in other words, the yaw and trajectory measured are the result of the net applied forces during the sabot discard. A simple model for the sabot discard force and moment system is proposed in this paper. A procedure for fitting differential equations, which is presented in Reference (4), is utilized to fit the data based on the proposed model. From the fit, the amplitude, duration, and direction of the discard loading can be extracted.

II. SABOT DISCARD FORCE AND MOMENT MODEL

The sabot discard is a very complex phenomenon because sabot petals are mechanically and aerodynamically separating from the penetrator. As the sabot/penetrator assembly exits the gun tube, there are mechanical decoupling forces between the gun and sabot, pressure loadings due to the reverse flow of the muzzle blast gases, and initial asymmetric lift-off of the petals due to residual elastic strain energy deposited during the inbore balloting motion. In the latter part of the transitional ballistic cycle, mechanical loads are generated as the sabots pivot on the penetrator body, and finally, hypersonic pressure and shock loads disturb the penetrator as the sabot petals fly in aerodynamic contact with the penetrator. This complex set of events occurs during the launch of a kinetic energy penetrator and usually causes the penetrator to alter its angular motion and center of gravity motion from the motion it had at the muzzle of the gun, see References (1) and (3). It is this change in the angular and linear dynamics of the penetrator that contains information about the discard loadings.

A simple model can mathematically describe the essence of the sabot discard phenomenon. The discard model is based on the free flight equations of motion for the penetrator with added terms for an impulsive loading. The model assumes that the penetrator would enter free-flight at the muzzle as if there were no discard disturbances and that the discard forces, whether mechanical or aerodynamic, can be modeled as an applied impulse occurring at some point in the transitional ballistic cycle. Muzzle blast disturbances will be ignored since they have been shown to be small and of short duration for most high-velocity penetrators, see Reference (5). Since most penetrators are de-spun in rifled tubes or launched from smoothbore tubes, it is assumed in the model that penetrator roll is sufficiently small that the motions in the vertical and horizontal planes are decoupled. With the latter assumptions it is only necessary to model the planar motion of a symmetric missile.

Consider the coordinate system along with the force and moment system presented in Figure (1). The earth-fixed inertial axes are marked with the subscript "e" and the body fixed axes are not subscripted. The body-fixed axes are coincident with the earth-fixed axes when the flight path angle θ is zero. The missile travels along a flight path with arc length s and the z_e earth-fixed axis is aligned with and positive in the direction of the gravity vector, g. The lift force, L, and drag force, D, are defined as usual, normal to and along the velocity vector, V, respectively. The static aerodynamic moment, M, has not been shown in Figure (1) for clarity. The impulsive discard force components $F_x(s)$ and $F_z(s)$ are applied at a distance aft of the penetrator center of gravity given by $\Delta X_{cg}(s)$. The discard forces result in a discard moment M(s). The discard force, moment, and point of application can be assumed to vary along the flight path.

For the purposes of this paper the analysis is simplified even further; it is assumed that only a mechanical disturbance occurs at the pivot point of the sabots on the penetrator. The pivot point is also assumed to be a constant distance aft of the center of gravity. The addition of an aerodynamic impulsive disturbance into the model requires a straight-forward extension of the equations. A second impulsive load applied at a different location on the penetrator must be added. The aerodynamic impulsive disturbance has been purposely omitted in this paper because including the extra terms only serves to complicate the mathematics and does not add to the essential features of the model.

The equations of planar motion resulting from the force system in Figure (1) are derived using the nomenclature, procedures, and small-angle assumptions described in Reference (6). The equations governing the yawing motion, the swerving motion (i.e., the transverse trajectory motion), and the longitudinal trajectory motion are given in Equations (1), (2) and (3):

$$\alpha'' - H\alpha' - M\alpha = \frac{C_M^*(s)}{k_t^2} + C_z^{*'}(s) \tag{1a}$$

$$H = \left(-C_{L_\alpha}^* + C_D^* + 2C_x^*(s) + \frac{C_{M_q}^* + C_{M_{\dot\alpha}}^*}{k_t^2} \right) \tag{1b}$$

$$M = \left(\frac{C^*_{M_\alpha}}{k_t^2} + C^{*'}_x(s) \right) \tag{1c}$$

$$\bar{z}''_e - (C^*_{z_q} + C^*_{z_{\dot{\alpha}}})\alpha' - (C^*_x(s) - C^*_{L_\alpha})\alpha = C^*_z(s) \tag{2}$$

$$\frac{V'}{V} = -C^*_D - C^*_x(s) \tag{3}$$

The gravity term has been ignored because it is negligible during the sabot discard sequence. The derivatives in the equations are with respect to the flight path coordinate **s** and all of the distances are normalized by the penetrator diameter. The forces and moments are in standard aerodynamic coefficient form; therefore, the forces are normalized by the dynamic pressure and reference area, **S**, (the penetrator cross-sectional area) and the moments by the dynamic pressure, the reference area, **S**, and the penetrator diameter, **d**. An example of the lift coefficient and the static moment coefficient is presented in equations (4) and (5).

$$C_L = \frac{\pm|L|}{\frac{1}{2}\rho V^2 S} \tag{4}$$

$$C_M = \frac{\pm|M|}{\frac{1}{2}\rho V^2 S d} \tag{5}$$

where a starred coefficient is defined as:

$$\{\}^* = \left\{ \frac{\rho S d}{2m} \right\} \{\}$$

The additional discard force and moment coefficients clearly stand out in the equations, since they are functions of the flight path coordinate (e.g.,$\mathbf{C_z^*(s)}$).

The objective of the analysis is to fit the above differential equation model to the data using a non-linear least-squares fitting technique presented in Reference (4); consequently a functional form for the discard loads must be prescribed. An analytic form for the impulse function was chosen to avoid infinite derivatives. The chosen functional form is a shifted sine wave. It is assumed the total discard force is applied on the outer surface of the penetrator at an angle ψ (measured positive counterclockwise) at the sabot pivot point, $\Delta \mathbf{X_{cg}}$. The impulse starts at position $\mathbf{s_i}$ on the flight path, has a path or discard length of $\mathbf{l_d}$ and an amplitude, **A**. The impulse function, the impulse force components and moment (in coefficient form) can be described by Equations (6), (7), (8), (9) and (10):

$$C^*(s) = \sqrt{C^*_z(s)^2 + C^*_x(s)^2} \tag{6}$$

$$C_x^*(s) = C^*(s)\cos\psi \tag{7}$$

$$C_z^*(s) = C^*(s)\sin\psi \tag{8}$$

$$C_M^*(s) = C^*(s)\{\sin\psi\Delta X_{cg} + \frac{\cos\psi}{2}\} \tag{9}$$

$$C^*(s) = A\{1 + \sin 2\pi(\frac{s - s_i}{l_d}) - \frac{\pi}{2}\} \tag{10}$$

$$C^*(s)\ is\ valid\ from\ s_f\ to\ s_i\ where\ s_f = s_i + l_d$$

All of the lengths in the equations have also been normalized by the penetrator diameter. In the governing equations the rate at which the impulse is applied also appears. The impulsive rate is obtained from Equations (6) through (10) by differentiating with respect to the path length. Note, both the impulse function and the angle of application vary along the flight path. A plot of the assumed total impulse and impulsive rate is given in Figure (2) for $\psi = \pi/2$.

If the free-flight aerodynamics of the penetrator are known or can be estimated then the non-linear fitting routine can be used to fit the governing Equations (1), (2) and (3) to data containing discard disturbances and in the process evaluate the unknowns in the assumed impulse function. The procedure, in the present case, would return values for the amplitude, A, the initial location of the impulse, s_i, the discard length, l_d, the initial angle of application, ψ_o of the discard force, and the rate of change of the angle of application, $\psi'(s)$,

III. DISCUSSION OF THE RESULTS

The most important effect of sabot discard disturbances is the deviation of the penetrator from its intended flight path and the increase in dispersion resulting from the deviation. The sabots also decelerate the penetrator while they are still mechanically coupled; however this deceleration only slightly reduces the subsequent free-flight velocity. This velocity reduction is not considered large enough to significantly affect the penetration performance. Therefore, only the transverse effects of the discard impulse will be retained for the purposes of the subsequent discussion.

The governing equations, (1) through (3), can be integrated numerically for an arbitrary impulse to gain insight into the behavior of the model. Consider applying a discard impulse normal to a penetrator, at the sabot pivot point, at a constant angle ($\psi = \pi/2$) to a 25mm penetrator such as discussed in Reference (7). The impulse starts at 2.0 metres, ends at 3.0

metres for a discard length of 1.0 metre and its shape and magnitude are given in Figure (2). The resultant yawing motion is presented in Figure (3). The solid line is the yawing motion that would have resulted had the projectile entered free flight at the muzzle without any disturbances. The dashed line is the yawing motion subsequent to the sabot discard impulse. A rather large impulse was applied but it serves to illustrate the effects clearly. The first maximum yaw has increased from approximately 3.5 degrees to 12 degrees and the location of the maximum yaw point has shifted downrange. The increase in first maximum yaw is directly proportional to the increase in the aerodynamic jump.

The force that caused this increase in yaw was applied aft of the center of gravity and in the given coordinate system is in the positive z direction. Figure (4) presents a similar comparison of the two swerve trajectories. The solid line is the swerve predicted if the penetrator enters free flight at the muzzle and the dashed curve is the swerve trajectory subsequent to the application of the discard impulse. Since the velocity vector is tangent to the swerve trajectory, the impulsive load has altered the direction of the penetrator center of gravity prior to free flight. This is the sabot discard jump discussed in References (3) and (7).

The latter predictions were for a mechanical sabot discard impulse applied normal to the penetrator axis. Data were acquired for a sabot/penetrator projectile such as the 120 mm cone-stabilized training projectile discussed in Reference (3). The data indicated that the largest sabot discard disturbance was from the mechanical disengagement of the sabot components. Figures (5a) through (5d) are a series of vertical x-ray images at stations one through four, respectively. The sabots mechanically disengage approximately 6 metres downrange of the muzzle, at the third x-ray station. By station four the sabots are almost out of aerodynamic contact with the penetrator and beyond this point the penetrator is in free-flight.

The governing equations were coded into the form required by the non-linear least-squares fitting routine, the data fitted and the yawing motion results are presented in Figure (6). The muzzle of the gun is located at -39.0 metres because the first spark shadowgraph station of the U. S. Army Transonic Range Facility is designated as the zero point. As in the previous predictions, the solid curve represents the yawing motion resulting from the yaw rate measured at the muzzle. The dashed curve is the non-linear least-squares fit of the equation with the assumed impulse function. The square symbols represent the x-ray data and the circular symbols represent the free-flight yaw measurements made in the first group of spark shadowgraphs. The dotted line is the yaw fit to the free-flight yaw data using the techniques described in Reference (6). Clearly the non-linear least- squares fit, based on the impulsive discard model proposed, captures the yawing motion at the muzzle and compares well with the free-flight motion and data measured independently of the x-ray data. The model fitted to this data assumed an arbitrary disturbance at an arbitrary location. The fit found the disturbance to occur near the third data point or at the third x-ray station. It is concluded that this disturbance is largely due to the mechanical sabot disengagement at that point, which can be identified as station three in the photographic data of Figure (5c). The sabots are still in aerodynamic contact until station four and are just over the fins at that location. Since the last two x-ray data points are free-flight data and are consistent with the Transonic Range free-flight data, it appears that the

aerodynamic discard disturbance was small relative to the mechanical disengagement disturbance.

The swerving motion results are plotted in the Transonic Range coordinate system in Figure (7), where the non-linear impulsive fit, given by the dashed line, compares very favorably with the x-ray data represented by the square symbols. The dotted line and circular symbols represent the Transonic Range free-flight swerve fit and data respectively. The solid line is almost identical in shape to the dashed line but it is displaced in the positive z_e direction. The fact that the curves are not coincident is probably due to a slight error in the meshing of the x-ray fiducial survey into the Transonic Range coordinate system resulting in an apparent displacement of the x-ray data in the positive z_e direction.

The non-linear least-squares fit returns values for the parameters A, S_i and I_d in Equation (10). The fit was made with $\psi = \pi/2$ so $C_z^*(s)$ is computed from Equation (8) and the discard force for this case is obtained by evaluating Equation (11):

$$F_z(s) = \{\frac{2m}{\rho S d}\} C_z^*(s) \frac{1}{2} \rho V^2 S \tag{11}$$

where **m** is the penetrator mass, ρ is the atmospheric density, **S** is the reference area, **d** the penetrator diameter and **V** the flight velocity. The peak force, average force, and impulse can be computed by the proper mathematical manipulation of Equation (11).

IV. CONCLUSIONS

A model based on the planar free-flight motion of a symmetric missile that incorporates an impulsive sabot discard load has been proposed. The model can be used to predict the effects of a transitional ballistic impulsive load on a sabot/penetrator launch or it can be incorporated into a non-linear least-squares fitting routine to extract impulsive loads from transitional ballistic data. The model, though simple, has been shown to adequately capture the basic mechanics of sabot discard disturbances and to provide reasonably good fits of transitional ballistic data. The discard loads derived from the data fits can be used to aid in the design of future sabot components and kinetic energy penetrators.

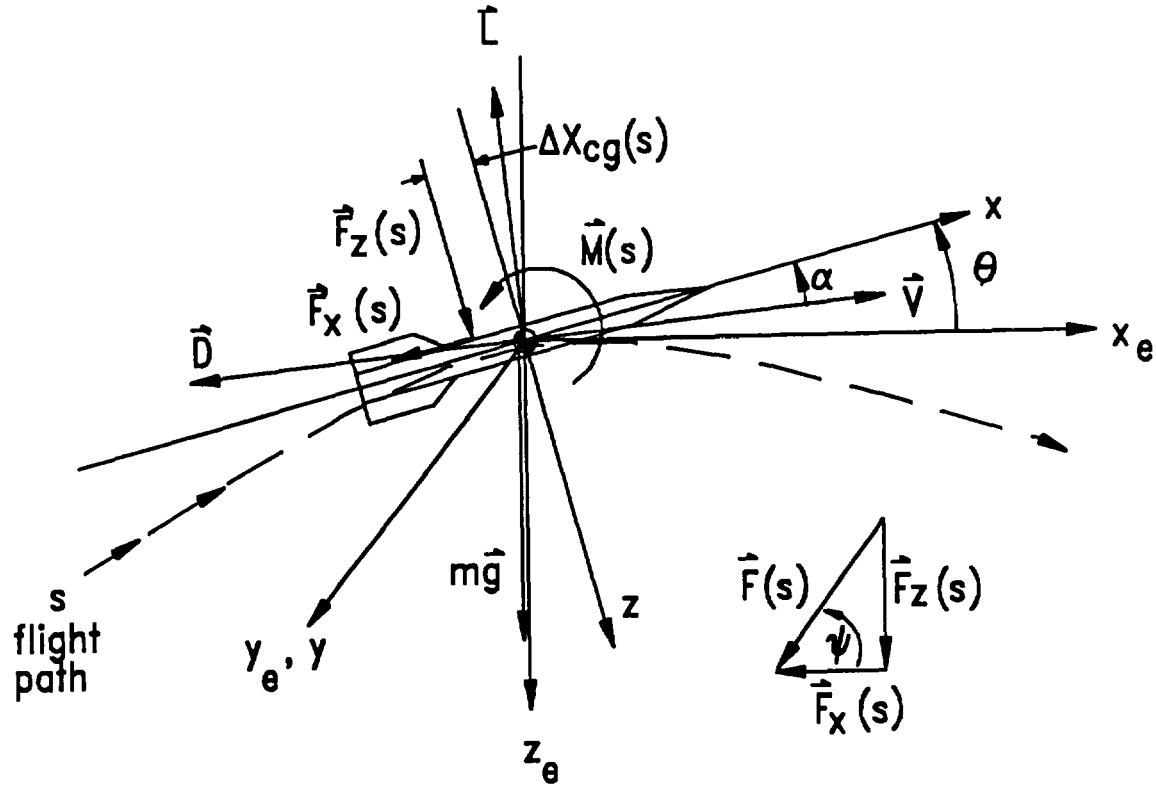

Figure (1) Discard Impulse Force and Moment Model and Coordinate System

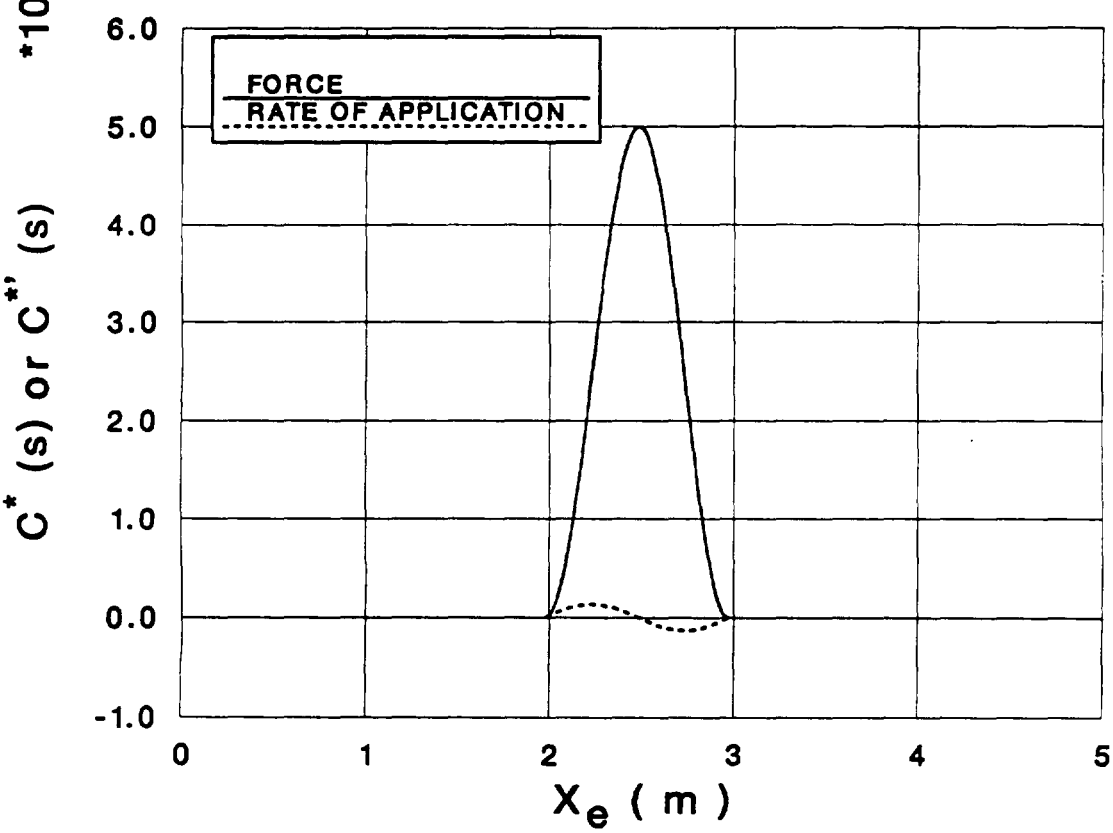

Figure (2) Assumed Impulse Function

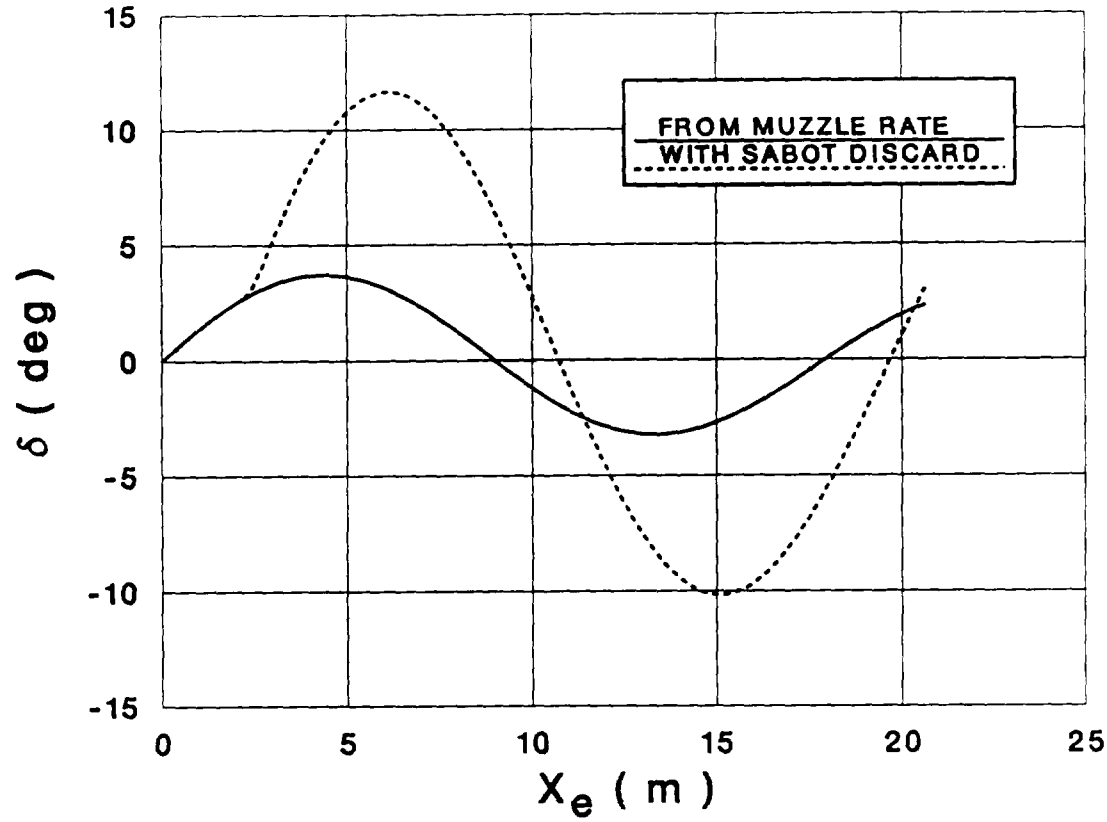

Figure (3) Predicted Yawing Motion: 25mm Kinetic Energy Penetrator

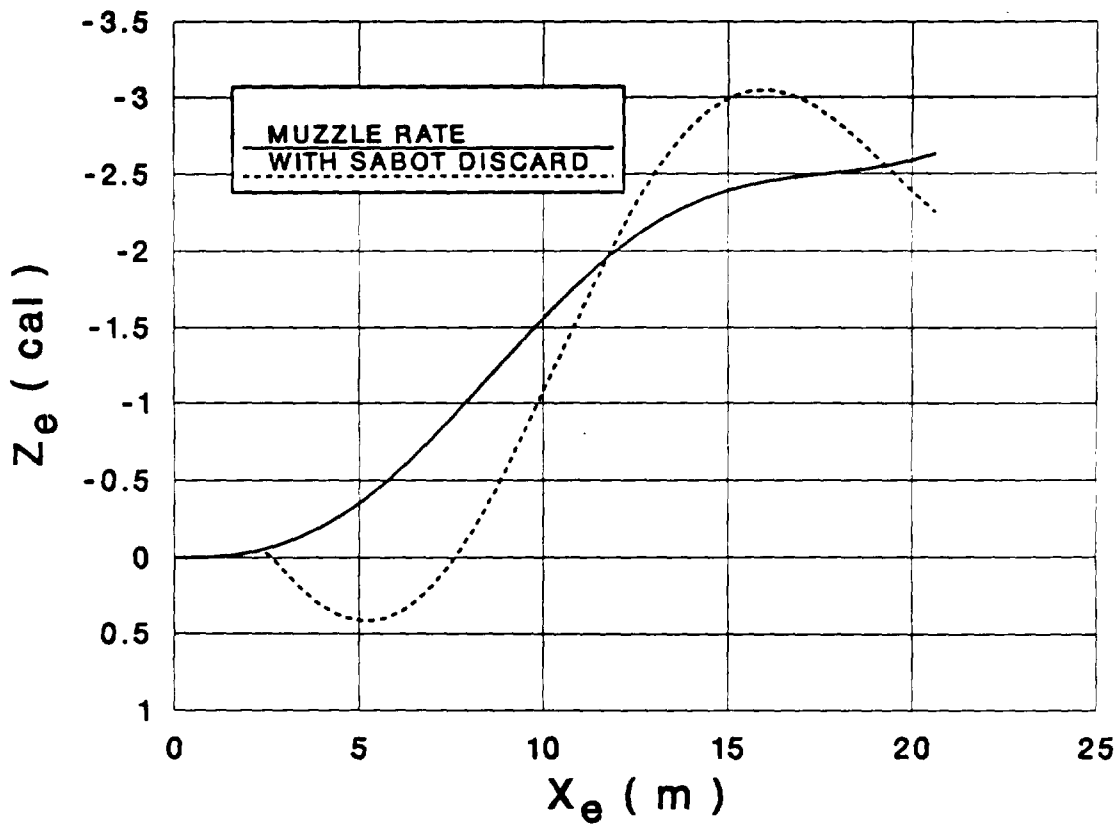

Figure (4) Predicted Swerve trajectory: 25mm Kinetic Energy Penetrator

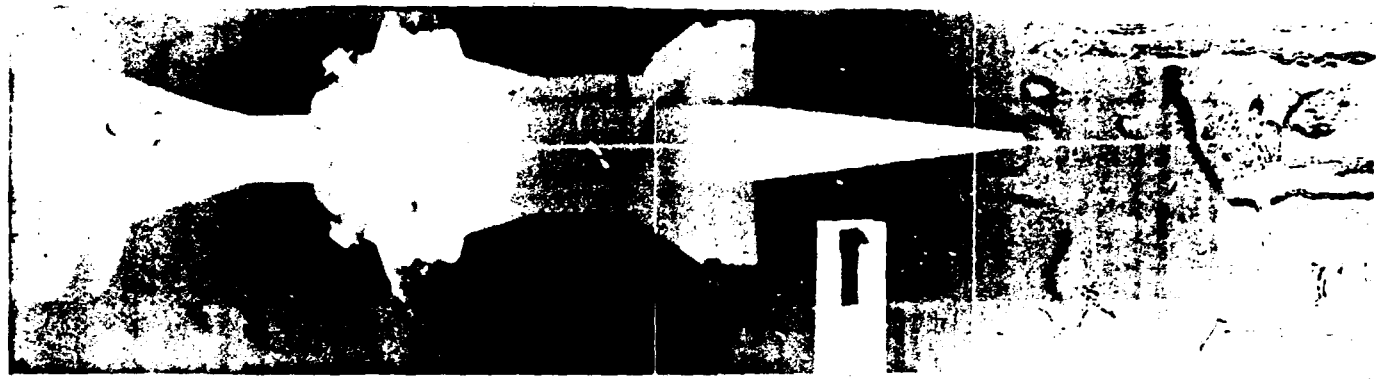

Figure (5a) Vertical X-Ray Image: Station #1

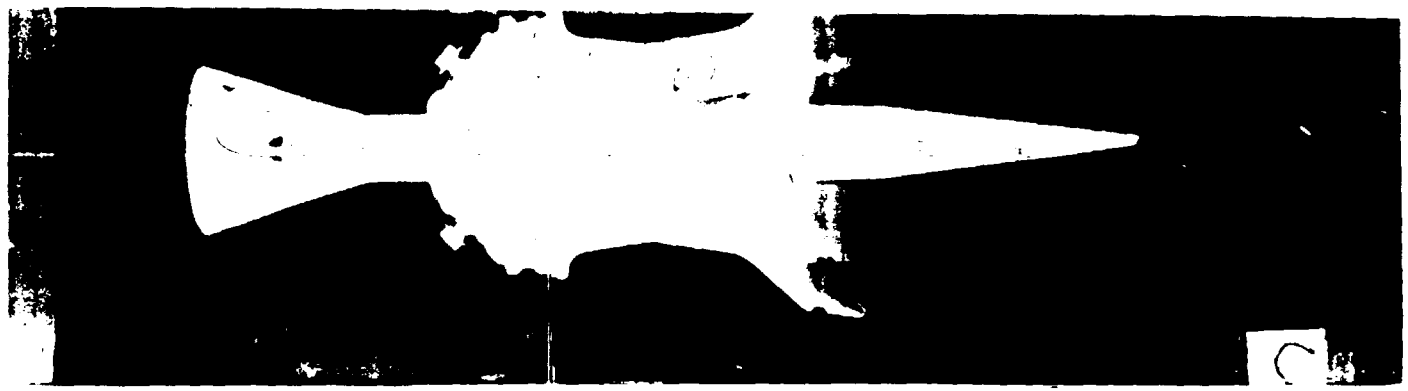

Figure (5b) Vertical X-Ray Image: Station #2

Figure (5c) Vertical X-Ray Image: Station #3

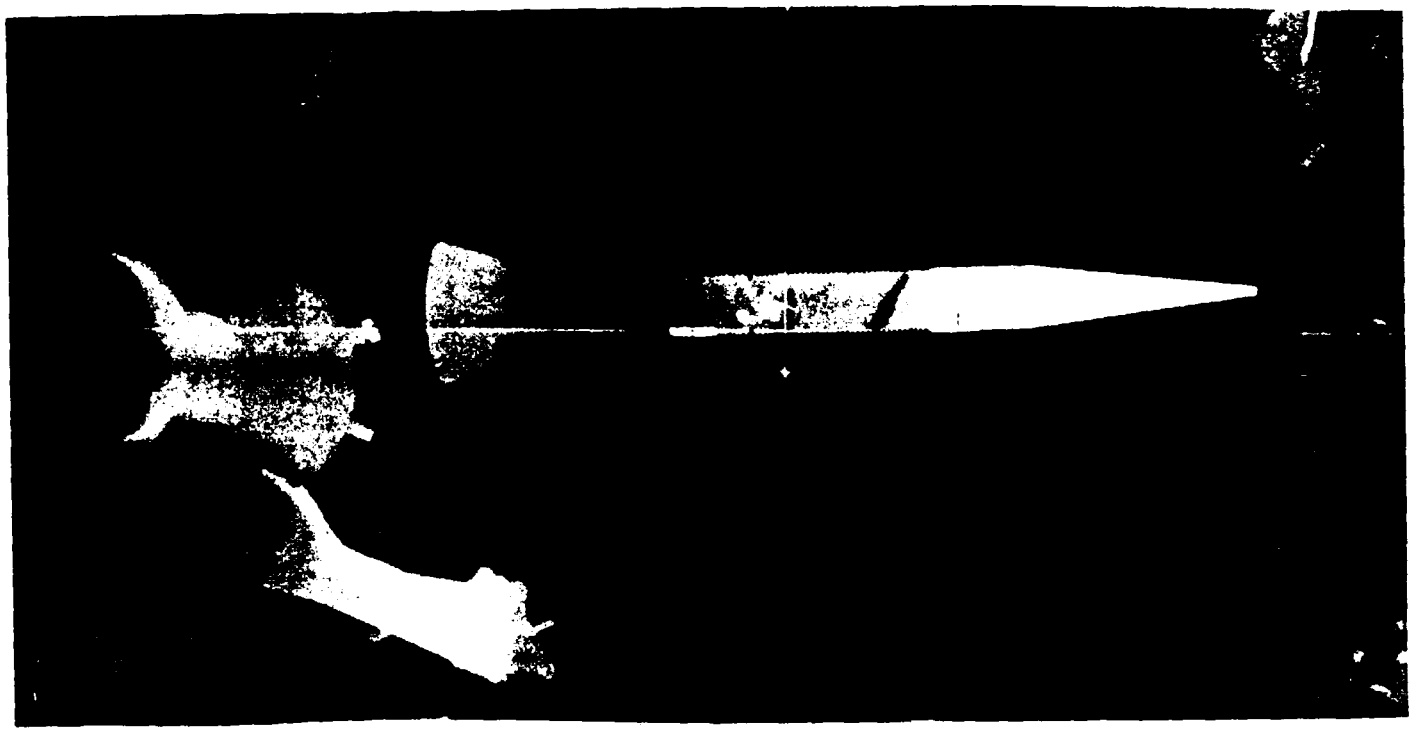

Figure (5d) Vertical X-Ray Image: Station #4

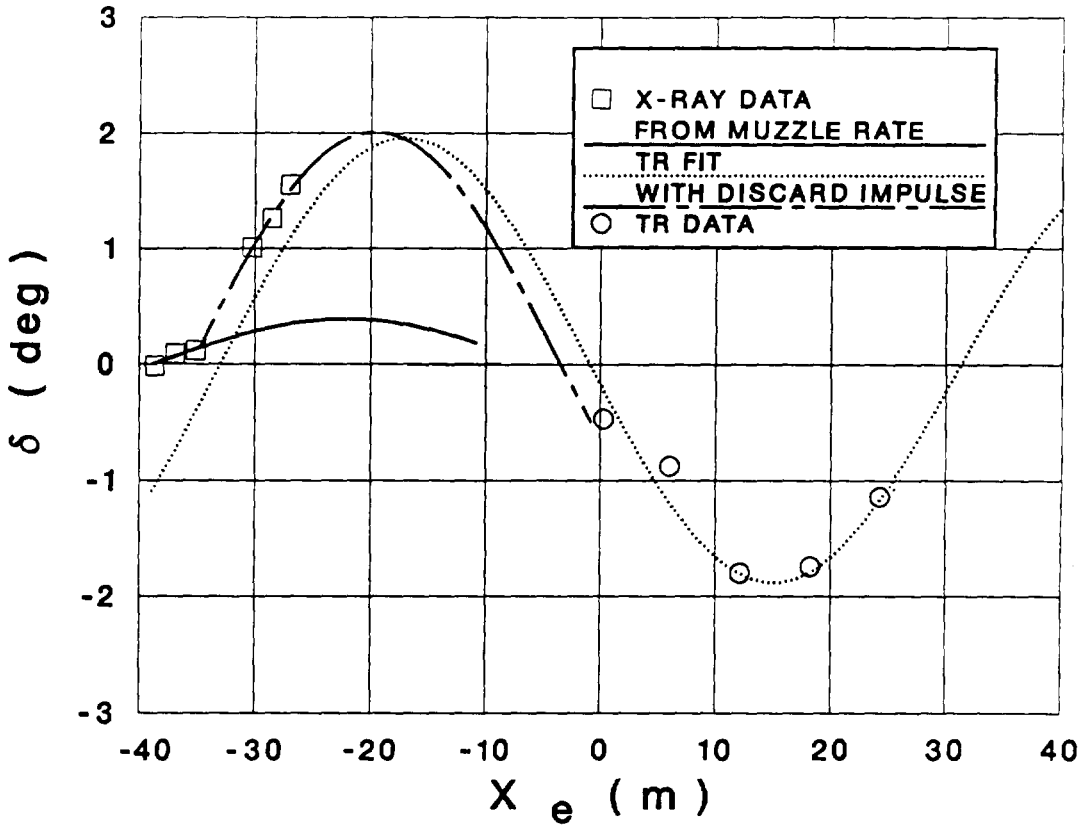

Figure (6) Fitted Yawing Motion: 120 mm Training Projectile

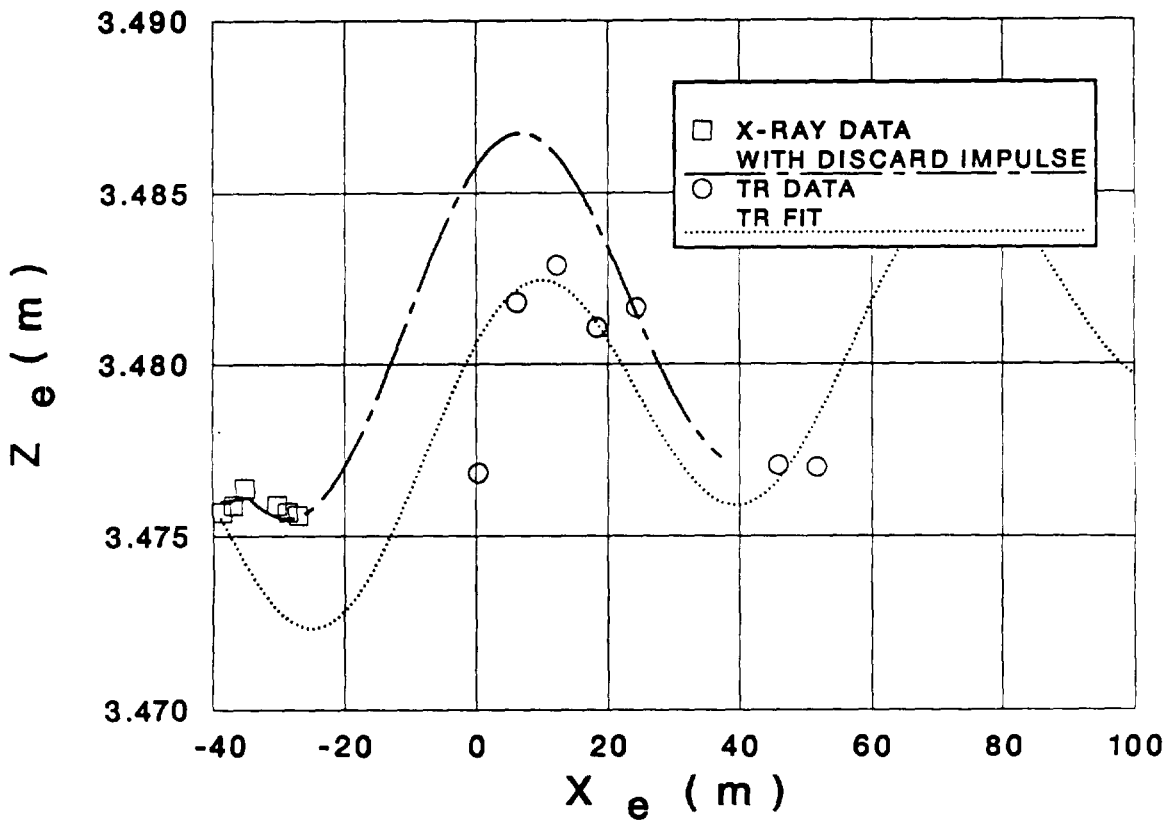

Figure (7) Fitted Swerve Trajectory: 120 mm Training Projectile

INTENTIONALLY LEFT BLANK.

VI. REFERENCES

(1) Plostins, P., "Launch Dynamics of APFSDS Ammunition," Proceedings of the Eighth International Symposium on Ballistics, American Defense Preparedness Association, Two Colonial Place, 2101 Wilson Boulevard., Suite 400, Arlington, Virginia 22201-3061, October 1984.

(2) Schmidt, E.M. and Shear, D.D., "Aerodynamic Interference During Sabot Discard," Journal of Spacecraft and Rockets, Vol.15, No.3, May-June 1978, pp.162-167, American Institute of Aeronautics and Astronautics, 370 L'Enfant Promenade S.W., Washington, D.C. 20024.

(3) Bornstein, J., Celmins, I., Plostins, P. and Schmidt, E.M., "Launch Dynamics of Fin-Stabilized Projectiles," AIAA-89-3395-CP, AIAA Atmospheric Flight Mechanics Conference, Boston, MA, August 1989, American Institute of Aeronautics and Astronautics, 370 L'Enfant Promenade S.W., Washington, D.C. 20024.

(4) Bradley, J.W., "FINLIE: A Fortran Program for Fitting Ordinary Differential Equations with Nonlinear Parameters to Data," ARBRL-TR-02290, U.S. Army Ballistic Research Laboratory, Aberdeen Proving Ground, Md. 21005-5066, February 1981.

(5) Schmidt, E.M., Fansler, K.S. and Shear, D.D., "Trajectory Perturbations of Fin-Stabilized Projectiles Due to Muzzle Blast," Journal of Spacecraft and Rockets, Vol.14, No.6, June 1977, pp.339-344, American Institute of Aeronautics and Astronautics, 370 L'Enfant Promenade S.W., Washington, D.C. 20024.

(6) Murphy, C.H., "Free Flight Motion of Symmetric Missiles," BRL-TR-1216, U.S. Army Ballistic Research Laboratory, Aberdeen Proving Ground, Md. 21005-5066, July 1963.

(7) Plostins, P., Celmins, I. and Bornstein, J., "The Effect of Sabot Front Borerider Stiffness on the Launch Dynamics of Fin-Stabilized Kinetic Energy Ammunition," Proceedings of the 11th International Symposium on Ballistics, American Defense Preparedness Association, Two Colonial Place, 2101 Wilson Boulevard., Suite 400, Arlington, Virginia 22201-3061, May 1989.

INTENTIONALLY LEFT BLANK.

No. of Copies	Organization
2	Administrator Defense Technical Info Center ATTN: DTIC-DDA Cameron Station Alexandria, VA 22304-6145
1	Commander U.S. Army Materiel Command ATTN: AMCDRA-ST 5001 Eisenhower Avenue Alexandria, VA 22333-0001
1	Commander U.S. Army Laboratory Command ATTN: AMSLC-DL 2800 Powder Mill Road Adelphi, MD 20783-1145
2	Commander U.S. Army Armament Research, Development, and Engineering Center ATTN: SMCAR-IMI-I Picatinny Arsenal, NJ 07806-5000
2	Commander U.S. Army Armament Research, Development, and Engineering Center ATTN: SMCAR-TDC Picatinny Arsenal, NJ 07806-5000
1	Director Benet Weapons Laboratory U.S. Army Armament Research, Development, and Engineering Center ATTN: SMCAR-CCB-TL Watervliet, NY 12189-4050
(Unclass. only) 1	Commander U.S. Army Armament, Munitions and Chemical Command ATTN: AMSMC-IMF-L Rock Island, IL 61299-5000
1	Director U.S. Army Aviation Research and Technology Activity ATTN: SAVRT-R (Library) M/S 219-3 Ames Research Center Moffett Field, CA 94035-1000

No. of Copies	Organization
1	Commander U.S. Army Missile Command ATTN: AMSMI-RD-CS-R (DOC) Redstone Arsenal, AL 35898-5010
1	Commander U.S. Army Tank-Automotive Command ATTN: ASQNC-TAC-DIT (Technical Information Center) Warren, MI 48397-5000
1	Director U.S. Army TRADOC Analysis Command ATTN: ATRC-WSR White Sands Missile Range, NM 88002-5502
1	Commandant U.S. Army Field Artillery School ATTN: ATSF-CSI Ft. Sill, OK 73503-5000
(Class. only) 1	Commandant U.S. Army Infantry School ATTN: ATSH-CD (Security Mgr.) Fort Benning, GA 31905-5660
(Unclass. only) 1	Commandant U.S. Army Infantry School ATTN: ATSH-CD-CSO-OR Fort Benning, GA 31905-5660
1	Air Force Armament Laboratory ATTN: WL/MNOI Eglin AFB, FL 32542-5000
	Aberdeen Proving Ground
2	Dir, USAMSAA ATTN: AMXSY-D AMXSY-MP, H. Cohen
1	Cdr, USATECOM ATTN: AMSTE-TD
3	Cdr, CRDEC, AMCCOM ATTN: SMCCR-RSP-A SMCCR-MU SMCCR-MSI
1	Dir, VLAMO ATTN: AMSLC-VL-D
10	Dir, BRL ATTN: SLCBR-DD-T

No. of Copies	Organization
5	Commander U.S. Army Armament Research, Development, and Engineering Center ATTN: SMCAR-CCL-CA, P. O'Neill C.A. Miller E. Malatesta G. Fleming Alan Li Picatinny Arsenal, NJ 07806-5000
4	Commander U.S. Army Armament Research, Development, and Engineering Center ATTN: SMCAR-AEI-A, R. Kline J. Grau Chiu Ng J. Whyte Picatinny Arsenal, NJ 07806-5000
1	Commander U.S. Army Armament Research, Development, and Engineering Center ATTN: AMSMC-QAF-S, D. Messer Picatinny Arsenal, NJ 07806-5000
3	Commandant U.S. Army Infantry School ATTN: ATSH-CD-MLS-S, SFC Kohlhase ATSH-INA-BPO, SFC Wood ATSH-TD-S-D, V. Hartman Ft. Benning, GA 31905-5800
1	Commander HQ, TRAC RPD ATTN: ATCD-MH, CPT J. Williams Ft. Monroe, VA 23651-5000
1	Commander U.S. Army Yuma Proving Ground ATTN: STEYP-MT-ET-C, W. Aynes Yuma, AZ 85365-9103
1	Commander Program Manager Bradley Fighting Vehicle System ATTN: AMCPM-BFVS, K. Pitco Warren, MI 48937-5000
1	Commander U.S. Army Armor Center & School ATTN: ATSB-SMT, MAJ Newlin Ft. Knox, KY 40121
2	Alliant Techsystems, Inc. ATTN: C. Rippe B. Becker 600 Second Street, NE Hopkins, MN 55343
3	Aerojet General Corporation ATTN: E. Daniels J. Parkinson S. Rush P.O. Box 296 Azusa, CA 91702
2	Arrow Tech Associates, Inc. ATTN: B. Whyte W. Hathaway P.O. Box 4218 South Burlington, VT 05401-0042
	Aberdeen Proving Ground
4	Dir, USACSTA ATTN: STECS-AA-LA, M. Maule J. Steier M. Feinberg A. Rose
1	Dir, USATECOM ATTN: AMSTE-TER, B. Marshall
2	Dir, USAMSAA ATTN: AMXSY-GI, D. Hartka CPT Klimack

USER EVALUATION SHEET/CHANGE OF ADDRESS

This laboratory undertakes a continuing effort to improve the quality of the reports it publishes. Your comments/answers below will aid us in our efforts.

1. Does this report satisfy a need? (Comment on purpose, related project, or other area of interest for which the report will be used.) _____

2. How, specifically, is the report being used? (Information source, design data, procedure, source of ideas, etc.) _____

3. Has the information in this report led to any quantitative savings as far as man-hours or dollars saved, operating costs avoided, or efficiencies achieved, etc? If so, please elaborate. _____

4. General Comments. What do you think should be changed to improve future reports? (Indicate changes to organization, technical content, format, etc.) _____

BRL Report Number BRL-TR-3244 Division Symbol _____

Check here if desire to be removed from distribution list. ____

Check here for address change. ____

Current address: Organization _____
Address _____
_____

DEPARTMENT OF THE ARMY
Director
U.S. Army Ballistic Research Laboratory
ATTN: SLCBR-DD-T
Aberdeen Proving Ground, MD 21005-5066

OFFICIAL BUSINESS

BUSINESS REPLY MAIL
FIRST CLASS PERMIT No 0001, APG, MD

Postage will be paid by addressee

Director
U.S. Army Ballistic Research Laboratory
ATTN: SLCBR-DD-T
Aberdeen Proving Ground, MD 21005-5066

NO POSTAGE
NECESSARY
IF MAILED
IN THE
UNITED STATES